Journal of Catalysis **205,** 147–156 (2002)
doi:10.1006/jcat.2001.3408, available online at http://www.idealibrary.com on IDEAL®

Linear Hydrocarbons Adsorbed in the Acid Zeolite Gmelinite at 700 K ab Initio Molecular Dynamics Simulation of Hexane and Hexene

L. Benco,*[,1] T. Demuth,* J. Hafner,* F. Hutschka,† and H. Toulhoat‡

*Institut für Materialphysik and Center for Computational Materials Science, Universität Wien, Sensengasse 8, A-1090 Wien, Austria;
†Totalfinaelf, Centre Européen de Recherche et Technique, B.P. 27, F-76700 Harfleur, France;
and ‡Institut Français du Pétrole, F-92852 Rueil-Malmaison Cedex, France

Received June 13, 2001; revised August 24, 2001; accepted August 24, 2001

First-principles molecular dynamics simulations are performed to sample the behavior of linear hydrocarbons within the acid zeolite gmelinite at high temperature. The analysis of the trajectories, the time-development of the bond lengths, and simulated IR spectra are presented for both neutral and protonated molecules. The acid proton shows no affinity toward paraffin and slightly increased affinity toward the double bond of the olefin. No spontaneous protonation of the olefin is observed. The simulation of the protonated linear C6H13+ molecule shows that the protonated species is stabilized within the zeolite framework, and no collapse to the neutral molecule occurs. No cracking or isomerization event is observed. The protonated molecule shows rather high mobility accompanied by a series of hydride transfers along the chain of the molecule. The transfer of the H atom leads to a relocation of the positive charge. The relocation is correlated to the position of the Al site in the zeolite framework. In the simulated IR spectra we observe no distinctive feature evidencing the existence of the protonated species.

1. INTRODUCTION

Zeolites are microporous aluminosilicates that have been widely used as acid–base catalysts (1–4). Industrial conversions using acid–base catalysts include processes like dehydration and condensation, cracking, isomerization, hydration, and hydrogenation (5). The conversions are chain reactions believed to follow the carbonium ion theory (6), and the positive charge of the carbocations is expected to be stabilized by long-range electrostatic interactions with the surrounding negatively charged zeolite framework. Detailed mechanisms of the elementary steps including initiation, propagation, and termination, are still unclear.

A cluster description of the acid sites in the zeolite is widely used to investigate the conversion of hydrocarbons (7–10). Calculated energy diagrams based on the static relaxation of atomic positions provide valuable information on the energy profile of the particular chemical reaction. The reaction path is chosen according to mechanisms proposed for the conversion of hydrocarbons on solid acids (11, 12), and the numerical procedure follows the minimum energy pathway. The behavior of the zeolitic system at finite temperature is simulated by techniques of molecular dynamics (MD) (13). The particles interact through a potential that, in most investigations, is taken as a sum of suitable pair potentials depending only on the distance between the particles. Such a simulation provides the dynamical properties of the zeolite framework and the adsorbed molecule and characterizes the adsorbent-to-adsorbate interaction (14). Overall agreement is achieved for transport and separation phenomena (14, 15). Full description of the catalytic conversion is possible, as well, but the reaction pathway must be known and the evaluation of the hypersurfaces must be performed by quantum mechanical methods (16).

Ab initio MD simulations of zeolites have been, due to large computational demands, applied only to simple phenomena such as the determination of the position of the countercations within the cages (17), hydration and ion-exchange processes (18), and adsorption of small molecules like water and methanol (19–24). In acid zeolites the water molecule adsorbs directly to the acidic proton. Proton exchange between the adsorbed water molecule and zeolite is found to mediate the proton transfer between O sites in both Na-free (25) and Na zeolites (26). The attempt to simulate zeolite-catalyzed methanol to gasoline (MTG) process, representing one of the simplest intrazeolite chemical reactions, demonstrates the enormous complexity of such a conversion (20, 27). Those applications show that realistic ab initio MD simulations of zeolites are too short to mimic the complete process of a chemical conversion.

In this work we use ab initio relaxation and MD techniques to study the conversion of the hydrocarbon molecule on the solid acid zeolite. The linear C6 hydrocarbon is chosen as a probe molecule that converts at high temperature via both cracking and isomerization mechanisms. Because the ab initio molecular dynamics is currently applicable only

[1] To whom correspondence should be addressed at Institute of Inorganic Chemistry, Slovak Academy of Sciences, Dubravska Cesta 9, Sk-84236 Bratislava, Slovakia. Fax: 431 4277 9514. E-mail: lubomir.benco@unlvie.ac.at.

0021-9517/02 $35.00

to relatively simple phenomena on the time scale of picoseconds, we decided for the following strategy. A series of short-term ab initio MD simulations is started at different stages of the conversion in order to sample the role of different factors supporting the reactivity. First, we investigate the dynamics of the proton attack at the adsorbed molecule and second, we explore the time evolution of the protonized molecule. The carbocation is expected to collapse at high temperature, thus forming products of the conversion. Our short-term MD sampling includes the effect of high temperature, and compares the behavior of saturated and unsaturated molecules and compares the effect of increased pressure of the feed molecules. Finally, the behavior of a carbenium ion within a zeolite at high temperature is tested with the example of protonated 3-hexene. The short-term simulations are expected to provide new details on the elementary steps of the conversion process and enhance the understanding of the elementary steps over which linear hydrocarbons in zeolites are either converted to isomers or cracked to smaller molecules.

2. STRUCTURAL MODEL

Simulation of the adsorption of hydrocarbons at high temperature is performed within the large pores of gmelinite (28). Gmelinite is not an industrial zeolite. The choice of gmelinite structure stems from the computational convenience (cf. Ref. (29)). The unit cell of gmelinite is medium sized. The total number of atoms per cell is 72, which is acceptable for demanding MD simulations. The cell dimensions are quite uniform, allowing insertion of molecules as large as *n*-hexane into the single unit cell. Finally this material has topological features, in particular hexagonal prisms, similar to those of faujasites, which belong to the most important industrial zeolites.

Purely siliceous gmelinite has the composition $Si_{24}O_{48}$ and forms a hexagonal structure with space group $P6_3mmc$. The secondary building block is a hexagonal prism whose parallel stacking leads to a columnar structure with prisms and large gmelinite cages alternating along each column (see Fig. 1). The largest channel is circumscribed by a ring of 12 SiO_4 tetrahedra (the 12-membered ring—12MR) extending along one dimension (the *c* axis). Each 12MR is interconnected to other three 12MRs through gmelinite cages. Access to the cage is possible through three 8MR from three different 12MRs (Fig. 1). The gmelinite cage and the hexagonal prism are also constituting elements of the crystal structure of industrially used zeolites. The largest aperture in the structure (12MR) is as large as ~7 Å. Due to the high space group symmetry all tetrahedral sites (Si/Al) are crystallographically equivalent and there are only four inequivalent O sites (numbered 1 to 4 in Fig. 1). X-ray structure refinement performed on natural gmelinite with a Si/Al ratio of approximately 2/1 and containing the corresponding number of counterions (typical composition $Na_8(AlO_2)_8(SiO_2)_{16}$) and a not very precisely

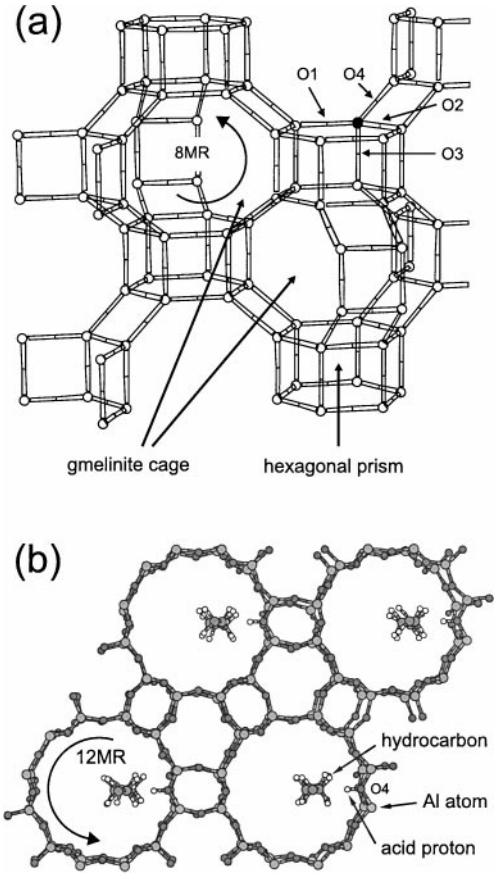

FIG. 1. Hexagonal structure of gmelinite. (a) The framework structure displaying the 8MR, the gmelinite cages, hexagonal prisms, and location of the O1–O4 sites, respectively. (b) Top view showing the large 12MR channels. The adsorbed linear molecule is extended along the main channel in the vicinity of the Brønsted acid site.

known number of water molecules (up to 24) yields the cell dimensions of $a = 13.756$ Å and $c = 10.048$ Å (Ref. (28)), corresponding to a volume of 68.59 $Å^3/SiO_2$-unit.

Simulations are performed using experimental unit-cell parameters (28), providing a unit cell volume slightly larger than the volume optimized using our computational approach (30). Experimental unit-cell volume thus reasonably corresponds with the volume slightly expanded at high temperature. The adsorbed linear molecules are inserted in the main channel extending along the *c* axis. The acidic proton resides at the O4 site, the O–H bond pointing to the center of the main channel. The molecule of the hydrocarbon is initially placed in the vicinity of the Brønsted acid site with a shortest O4-to-C contact of ~2.0 Å (cf. Fig. 1). A second hydrocarbon molecule is placed in the main channel behind the first one, keeping a parallel orientation relative to the channel.

3. COMPUTATIONAL DETAILS

Ab initio molecular dynamics simulations for characterizing the dynamical properties of the hydrocarbon

containing zeolites are performed. The calculations are based on density-functional theory (31) using the generalized-gradient approximation (32) to the exchange-correlation functional. We use the ultrasoft pseudopotentials (33, 34) and a plane-wave basis as implemented in the Vienna ab initio simulation package VASP (35). The calculations are performed using Blöchl's projector augmented wave (36, 37) technique with a plane-wave cutoff energy of 300 eV. Brillouin-zone sampling is restricted to the Γ point. Convergence is improved using a modest smearing of the eigenvalues. Fixed-volume molecular dynamics simulation is performed at 700 K. The dynamics uses the exact Hellman–Feynman forces acting on atoms, and applies the statistics of the canonical ensemble to the motion of atomic nuclei (38) and the Verlet velocity algorithm [13] with a time step for the integration of equations of motion of $\Delta t = 1.0$ fs. The frequency bands are calculated via the Fourier transform of the velocity autocorrelation function. The simulation times are $\sim$3 ps. The frequency of the heat bath is tuned to that of the O–H bond to support the mobility of the acid proton.

All configurations for which molecular dynamics is started are preoptimized using static relaxation of all atomic positions. The relaxation releases local deformations and stresses that could contaminate atomic velocities at the beginning of the simulation and could lead to unnatural behavior. The dynamics is then started from such a configuration that slightly differs from the completely optimized atomic positions. The choice of optimized positions could cause during the short-term dynamics some vibrational modes to fail to develop.

4. RESULTS AND DISCUSSION

The ab initio molecular dynamics simulations at the temperature $T = 700$ K are performed with both the neutral molecules and the carbenium cation formed by the transfer of the acid zeolitic proton to the double bond of the unsaturated molecule.

4.1. Neutral Molecules

The simulation of the adsorption of neutral molecules in a zeolite are performed with one molecule of *n*-hexane per unit cell and with different concentrations of 3-hexene corresponding to one, two, and three unsaturated molecules per unit cell.

Binding energies. Interactions between the hydrocarbon molecule and the zeolite framework are weak and nondirectional and the interaction energy comprises a high percentage of dispersion energy. The density-functional theory (DFT) with the generalized gradient approximation (GGA) for the exchange functional includes only a small fraction of dispersion forces (39, 40). Calculated interaction energies of saturated hydrocarbons in zeolites are therefore too small. Our recent paper (41) reports the interaction energies in gmelinite for C4–C6 hydrocarbons as a function of the concentration of acid sites. For *n*-hexane adsorbed at the acid site we obtain 16.4 kJ/mol. No adsorption energies of hydrocarbons are available for gmelinite. An interpolation of values measured in zeolites with different framework density (42) indicate for *n*-hexane the value of $\sim$65 kJ/mol. The large difference between $\sim$16 and $\sim$65 seemingly disqualifies our calculational method from applications to the adsorption of hydrocarbons in zeolites. Recently Eder and Lercher [43] have evaluated the contribution of the acid site to the heat of adsorption in zeolites MFI and FAU. Reported values of $\sim$7 kJ/mol (FAU) and $\sim$10 kJ/mol (MFI) are independent of the length of the hydrocarbon chain. Our calculated contribution of the acid site to the interaction energy provides the value of 12.3 kJ/mol (16.4 minus 4.1 kJ/mol calculated for the adsorption in the purely siliceous structure, cf. (41)) in good agreement with experimental data by Eder and Lercher (43). It is still unclear how to characterize dispersion contributions to the binding energy of hydrocarbons. Because of the spherical nondirectional character of such interactions we suppose that dispersion forces only decrease the mobility of adsorbates and products and cannot influence reaction pathways. For the interaction with the acid site our computational method provides the correct value. It is therefore a proper tool to characterize the interaction between the hydrocarbon molecule and a reaction center of the zeolite.

The interaction energy calculated for 3-hexene of 17.0 kJ/mol is similar to that of *n*-hexane (16.4 kJ/mol, cf. above). The presence of a single double bond does not increase considerably the interaction energy between the acid site and the hydrocarbon molecule. A different behavior has been observed for aromatic hydrocarbons. For benzene adsorbed at the acid site in mordenite, Demuth *et al.* calculated the interaction energy of $\sim$50 kJ/mol (44), which is approximately three times higher than that with linear molecules of hexane and hexene. The calculated interaction energies of hexene and benzene are in contradiction with the conclusions of the FTIR study by Trombetta *et al.* (45). For *n*-butenes adsorbed at the acid site of HZSM5 they observe a shift of the OH stretching frequency of $\sim$600 cm^{-1}, much higher than that of benzene of $\sim$350 cm^{-1}. In conclusions they state accordingly that a strength of the O–H hydrogen bonding toward an adsorbed hydrocarbon molecule is higher for butenes than for benzene. More comments on this discrepancy are given below in the paragraph with calculated O–H stretching frequencies.

Trajectories. Predominant movement of the single *n*-hexane molecule is in the lateral direction and only a small shift along the *c* direction is observed during the simulation. The trajectories are therefore represented as lateral interatomic distances between the active site of the zeolite (cf. position of the O4 atom in Fig. 1) and the C atoms

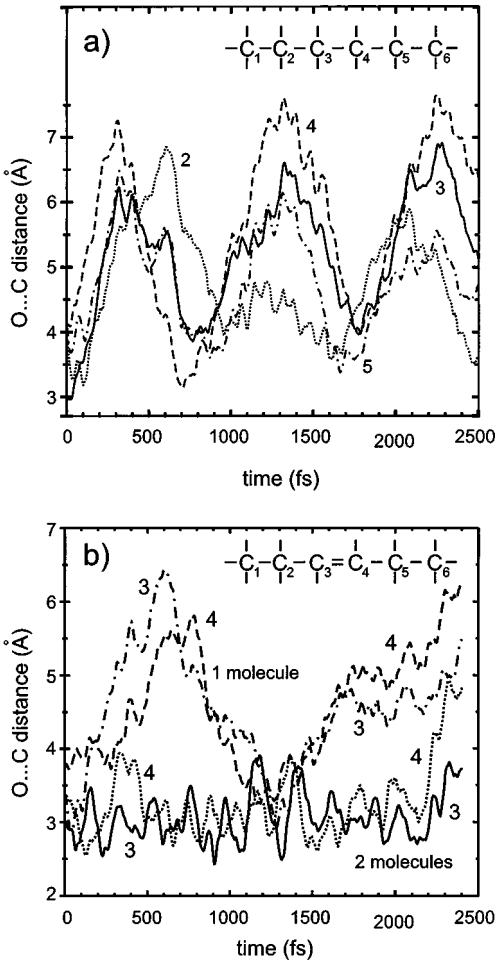

FIG. 2. Trajectories of neutral molecules adsorbed in the zeolite at high temperature: (a) hexane and (b) 3-hexene.

of the hydrocarbon molecule and are displayed in Fig. 2. The top panel shows the trajectory of *n*-hexane, displaying the distances between the O4 atom of the zeolite framework and the C atoms of the molecule with exclusion of the two C atoms of the terminal CH_3 groups. Four curves are designated 2–5 according to the numbering of the C atoms in the inset. The periodicity of curves indicates that the saturated molecule is reflected periodically between the walls of the zeolite channel with a period of ∼500 fs. The shortest O-to-C contacts of ∼3.2 Å correspond to ∼2.2 Å between the acid H atom and the C atoms of the hydrocarbon. Such a distance corresponds to a weak hydrogen bond (46). A saturated molecule adsorbed at high temperature in a zeolite thus shows rather inert behavior, making only weak contacts to the acid site.

The bottom panel of Fig. 2 shows the trajectories of 3-hexene at two different concentrations. Displayed curves show distances from the active site O4 of the zeolite to the C_3 and C_4 atoms involved in the double bond, which is the most reactive center on the adsorbed molecule. For a single molecule only one close contact following that of the starting configuration is observed after ∼1200 fs. The increased period of time between the two contacts and irregularities in the shape of curves indicates that the motion of the unsaturated molecule is more complex than that of the alkane. The contacting O-to-C distances of ∼3.0 Å are shorter than those of the saturated molecule (cf. Fig. 2a) but the corresponding H-to-C distance of ∼2.0 Å is still too large for effective attack of the acid proton at the double bond of the hydrocarbon molecule. Surprisingly, the time interval during which the molecule is in a tight contact with the active site of the zeolite of ∼200 fs is not longer than that of the saturated molecule.

Two lines at the bottom of Fig. 2b show trajectories for the case of two 3-hexene molecules per cell. Distances are displayed for the molecule situated closer to the active site. Increased pressure causes that the double bond of one molecule to stay in a tight contact with the acid site and some O-to-C distances are as short as 2.5 Å. One short-time transfer of the acid proton to the hexene molecule is observed during the simulation (not displayed). Despite the increased pressure the acid proton resides at the zeolite framework and no real activation of the hydrocarbon molecule is observed.

Bond lengths. Figure 3 shows the C–H and C–C interatomic distances as a function of time. The three lines in Fig. 3a represent a bond from the terminal CH_3 group and from two different CH_2 groups. The bond lengths vary between ∼1.02 and ∼1.23 Å, the largest amplitudes being observed for the CH_3 group. The frequencies of bonds within the CH_2 groups are similar and slightly smaller than that of the CH_3 group.

While the C–H bonds accomplish simple harmonic stretching, which is by symmetry independent of other vibrations, the time development of the C–C bonds shows a more complex pattern. The lines displayed in Fig. 3b for three distinct bonds show considerable modulation of the stretching with other vibrational modes. The C–C distances vary between ∼1.44 and ∼1.64 Å.

Figure 4 shows the time development of the C–C distances in 3-hexene. For the double bond the distance ranges from ∼1.32 to ∼1.42 Å and is clearly distinguished from simple bonds. The distances of the simple bonds are similar to those in the saturated hydrocarbon (cf. Fig. 3b).

IR spectra. Figure 5 compares the experimental gas-phase IR spectrum of hexane (47) and our simulated vibrational states derived from the dynamics of hexane at 700 K. The dominating feature in the experimental spectrum is the intense band of the C–H stretching modes centered at ∼2900 cm^{-1} with the maximum at ∼2960 cm^{-1} and a low-frequency subband at 2890 cm^{-1}. Two weaker bands at 1440 and 1380 cm^{-1} originate from the asymmetric and symmetric C–C stretching, respectively. States below 1200 cm^{-1} are due to deformation modes of the C–C and

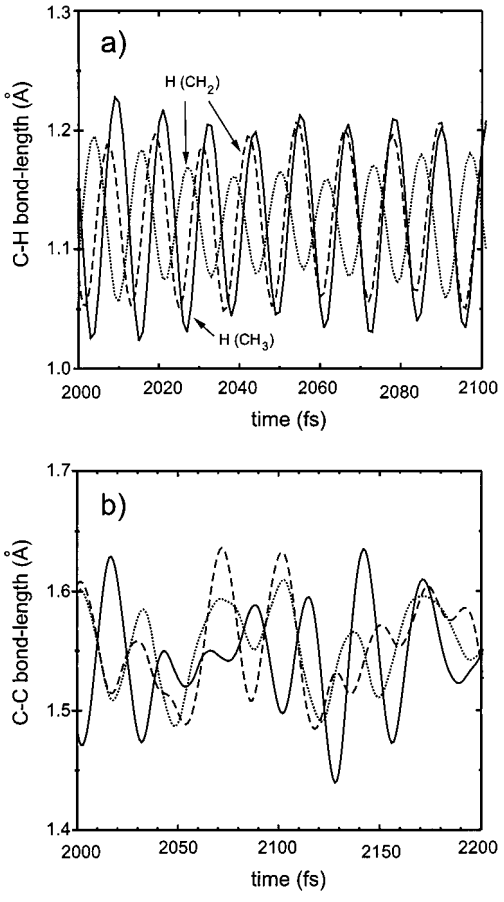

FIG. 3. Time dependence of the interatomic distances in *n*-hexane. (a) C–H distances displayed for one bond on C_1 (solid), C_2 (dashed), and C_3 (dotted). (b) C–C distances displayed for C_1–C_2, C_2–C_3, and C_3–C_4 bonds, respectively.

C–H bonds. The simulated spectrum (Fig. 5a) shows the C–H stretching band centered at ∼2860 cm^{-1} and a broad-band of unresolved states spread up to ∼1500 cm^{-1}, which comprise both the C–C stretching of the hydrocarbon and

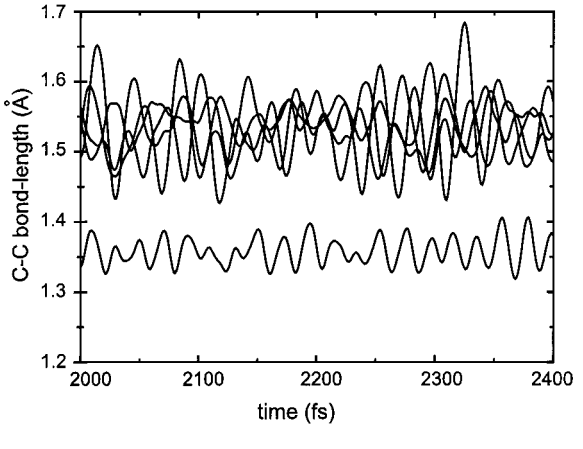

FIG. 4. Time dependence of the C–C distances in 3-hexene.

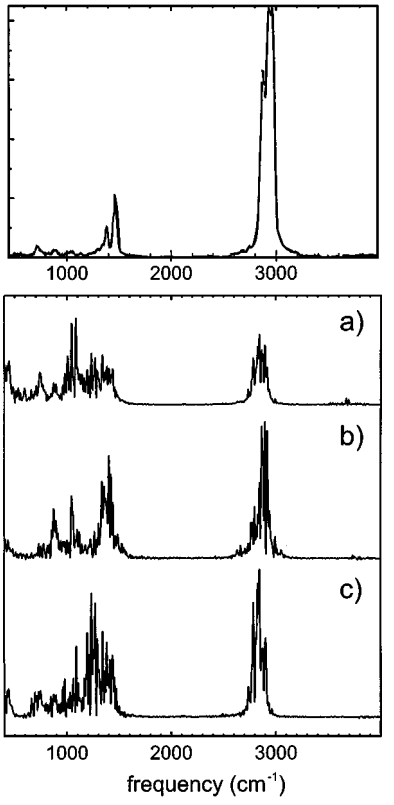

FIG. 5. IR spectra of hexane. (Top panel) Experimental gas-phase spectrum. (Bottom panel) Simulated spectrum of hexane adsorbed in the zeolite. (a) Total density of the vibrational states. (b) The states of the H atoms of the CH_3 groups. (c) The H-projected states of the CH_2 groups.

the skeletal vibrations of the zeolite framework. The location of the C–H stretching bands agrees reasonably with the experimental stretching modes. The projection of the states onto the H atoms of the CH_3 and CH_2 groups are displayed in Figs. 5b and 5c, respectively. The projections show that two components of the band can be distinguished in good agreement with two maxima in the experimental spectrum. The higher frequencies originate in the stretching within the CH_3 groups and the low-frequency components stem from the CH_2 groups, in good agreement with the accepted assignment of the C–H stretching bands.

The simulated bands of the O–H stretching of the zeolitic Brønsted acid site are displayed in Fig. 6. The band of the adsorbate-free zeolite is centered at ∼3810 cm^{-1}. The Fourier-transformed frequencies are known to result in O–H stretching, the modes of which are ∼200 cm^{-1} higher than experimental values, reflecting a certain overestimation of the O–H bond strength. The calculated frequency thus corresponds to that of the Brønsted acid site of ∼3610 cm^{-1} (48, 49). The adsorption of both hexane and hexene lowers the O–H stretching frequency (Fig. 6) by approximately the same value. The downshift of ∼180 cm^{-1} indicates that the contact of the absorbed molecule to the acid hydrogen is weak and qualitatively similar for

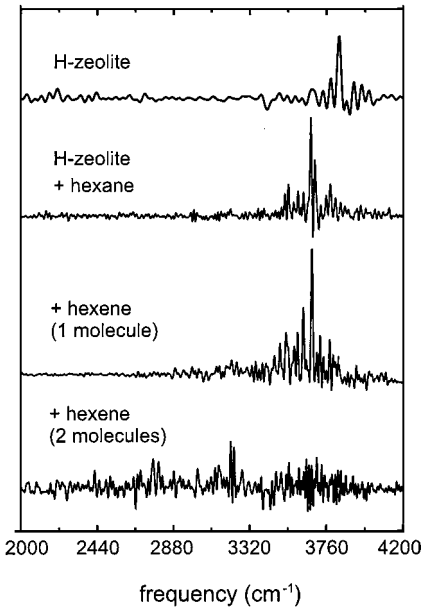

FIG. 6. O–H stretching bands of the adsorbate-free acid zeolite (top) and zeolites with adsorbed hydrocarbons.

both paraffin and olefin molecules. Measured shifts of the O–H stretching bands depend on the concentration of the adsorbed hydrocarbon. For *n*-pentane of HZSM5 a shift of ~100 to ~150 cm^{-1} is observed (48). Shifts ranging from ~105 to ~115 cm^{-1} are measured for *n*-hexane on H-FAU, H-MFI, and H-MOR (50). No similar measurements on gmelinite are reported, but our calculated shifts are in reasonable agreement with data available on other zeolite structures (48, 50).

Dynamical behavior of the hexane and hexene molecules adsorbed in gmelinite shows many similarities. Both molecules are located mainly in the center of the channel, making only weak contacts with the walls of the zeolite framework. The time interval during which either molecule is in a "tight" contact with the active site is also similar (~200 fs). It is therefore not surprising that Fourier-transformed O–H stretching frequencies are for both molecules downshifted by a similar value of ~180 cm^{-1}. In contrast surprising is the observation by Trombetta *et al.* (45) that the downshift due to the adsorption of butenes in HZSM5 is as large as ~600 cm^{-1}. Their value observed for benzene of ~350 cm^{-1} is in good agreement with our downshift of 317 cm^{-1} calculated for mordenite (44). We therefore suggest the authors to reconsider their interpretation and focus their attention on a band near 3520 cm^{-1} (*n*-butene) and near 3500 cm^{-1} (iso-butene). These well-visible bands are, in their spectra, left uninterpreted (Fig. 4 in Ref. (45)). Our calculated stretching frequencies indicate that these bands correspond with the downshifted frequencies induced by hydrogen bonding of the adsorbed olefins.

A high pressure of the adsorbed molecules leads to a tight contact between the molecule and the acid site as observed for two molecules of hexene per cell. Figure 2b shows that the average O-to-C distance is shorter than 3 Å. The acid H atom makes three different contacts to the olefin molecule. (i) The contact to the C atoms of the double bond is stabilizing; i.e., the O–H group points directly to the C atom. The O–H distance is considerably elongated or a short-term proton transfer to the C atom occurs. (ii) The contact to the π electron density of the double bond is only slightly stabilizing. (iii) Finally, the contact to the H atoms of olefin is destabilizing; i.e., the H atoms show a tendency to avoid each other. Both stabilizing and destabilizing contacts induce deformations of the acid site, leading to considerable deviations of the O–H bond from the equilibrium orientation. The shortest distances between the acid site and the olefin molecule are during the short-term contacts as short as 1.4 Å (not displayed in Fig. 2b).

The O–H stretching frequencies at high pressure of olefin molecules are displayed at the bottom of Fig. 6. The spectrum is much more noisy than the previous curves. In adsorbate-free zeolite and with a single adsorbed molecule the vibration motion of the O–H group is equilibrated. At high pressure the tight contact with atoms of the closest adsorbed molecule induces the alteration of different bonding situations (bonding/antibonding). The acid proton is frequently forced to change position. Despite the fact that it is not permanently transferred away from the zeolite framework, no distinct O–H stretching band is observed in the IR spectra (Fig. 6, bottom). The stretching frequencies are scattered over an interval larger than 1000 cm^{-1} and downshifted from the frequency observed at low pressure. No IR stretching bands are therefore expected in high-pressure adsorption experiments on H forms of zeolites.

4.2. Protonized Molecule

Simulations of adsorption at the temperature of 700 K are performed with stoichiometric gmelinite with an acid proton located at the O4 site. Under these conditions no effective proton transfer to the double bond of the unsaturated hydrocarbon is observed. The behavior of the protonated species in the zeolite surroundings is, however, of considerable interest. They represent intermediates of intrazeolite conversions, and in particular cases the protonated species are detected as relatively stable entities (51, 52). The understanding of reaction channels leading to the formation and stabilization of such species can shed more light on the intrazeolite chemistry. We therefore transfer the zeolite acid proton artifically to the double bond of the linear molecule of 3-hexene, thus creating a secondary carbenium cation. When the carbenium cation is left in the same position as obtained for the relaxed neutral physisorbed molecule the fast collapse occurs during the first steps of the dynamics. The proton is transferred back to the zeolite framework,

thus restoring the neutral physisorbed complex. We therefore place the protonated molecule in the center of the channel at an O4-to-C distance larger than 4 Å (cf. Fig. 1). After relaxation of all atomic positions such a cation is by ~60 kJ/mol less stable than the neutral molecule adsorbed to the acid site. The disadvantage of such a protonation explains why the proton does not attack the double bond, and the energy difference is too large to be overcome by thermal energy at high temperature.

Trajectories. The MD simulations of the carbenium cation inside the negatively charged zeolite framework show that the protonated molecule in zeolite surroundings is long-lived. Long-range electrostatic interactions stabilize the cation, and no collapse to a neutral molecule and an acid zeolite are observed. The protonated molecule remains extended along the main channel, slightly off-center from the location of the Al site. Compared to the neutral molecule the cation is more mobile and moves both horizontally and vertically. Much larger deformations of the molecular chain are also observed. The MD trajectories are shown in Fig. 7. The displayed curves indicate the distance between the O4 atom of the framework and the C atoms of the molecule (labeling of atoms and curves as in the inset). No periodicity as in the case of the saturated molecule has been observed. The continuous increase of all distances, which occurs after ~1.5 ps, is due to the vertical movement of the carbocation along the main channel. Interestingly, the O4-to-C distances of ~2.8 Å are similar to those observed for the neutral molecule at high pressure (cf. Fig. 2b), but this does not lead to the back-transfer of the proton to the zeolite framework. After the carbocation is located in the stabilized position in the center of the channel it seemingly does not act as a Brønsted acid. The proton attracts the electron density of the double bond, thus creating a regular H–C bond and a positive charge located at the other C atom of the double bond.

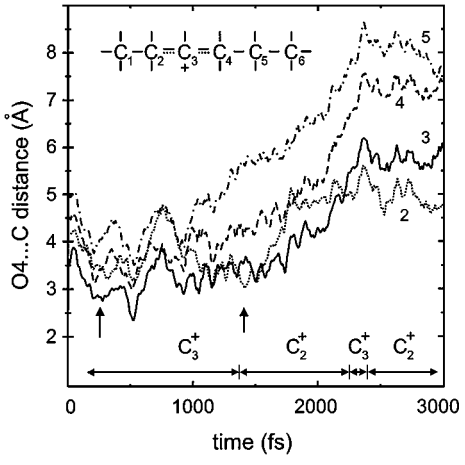

FIG. 7. Time dependence of the distance between the zeolite framework and the adsorbed protonated molecule. The location of the positive charge is indicated by horizontal arrows at the bottom of the figure.

An interesting phenomenon accompanying the movement of the carbocation in the zeolite channel is the migration of the hydride atoms along the molecular chain. It is accomplished in such a way that the H atom in the position neighboring the location of the positive charge jumps to the C^+ atom together with the electron density of two electrons. The hydride transfer thus leads to a shift of the positive charge to the neighboring C atom. The starting location of the positive charge is on the C_3 atom as indicated in the inset of Fig. 7. During the simulation three transfers of the hydride atom are observed. The lifetime of each protonated form is indicated by horizontal arrows at the bottom of the figure. The positive charge on the molecule is mobile and seems to be correlated with the negative charge fixed to the O atoms surrounding the Al site. The driving force behind the mobility of the positive charge is its effective interaction with the framework and the proper distance between the charges is tuned by shifting the hydride atoms. The distances displayed in Fig. 7 show that at the beginning of the simulation the shortest distance is observed for the C_3 atom and corresponds to the C_3^+ location and at the end the C_2^+ location correlates with the shortest O_4-to-C_2 distance. Two positions of the protonated molecule relative to the framework and corresponding locations of the positive charge are displayed in Fig. 8. Two different locations relative to the framework occurring after a short simulation time of ~1 ps demonstrate high mobility of protonated species. Figure 8 also shows that a considerable deformation of the linear molecule occurs.

Bond lengths. Figure 9 displays the C–H interatomic distances of the H_1 and H_2 atoms of the carbocation (cf. inset). The distances show two hydride transfers occurring at ~2230 and ~2380 fs of the simulation. At the beginning the H_1 atom is bound to the C_3 atom with a bond length oscillating around ~1.13 Å (a). This bond length of the protonated molecule is similar to those observed in the neutral molecule (Fig. 3). Upon the jump of H_1 to the neighboring C_2 atom the distance to the C_1 atom increases and the distance to the C_2 atom decreases to the value of the bond length (b). The positive charge is thus relocated from C_2 to C_3. Shortly later at ~2380 fs, H_2, residing on the C_2 atom, jumps back to the C_3 atom (c, d), thus returning the positive charge to the C_2 atom.

In Fig. 10 the C–C bond distances are displayed on the same time scale as that of Fig. 9. Three lines indicate one simple C–C bond and two C–C^+ bonds formed upon protonation of the double bond (labeling as in insert). Clear differences in the bond length are observed for the two types of bonds. The mean value of ~1.53 Å around which the bond distance of the simple bond oscillates agrees well with the bond length from the static optimization of the molecule *in vacuo* of 1.528 Å (41). The C–C^+ bond distances are

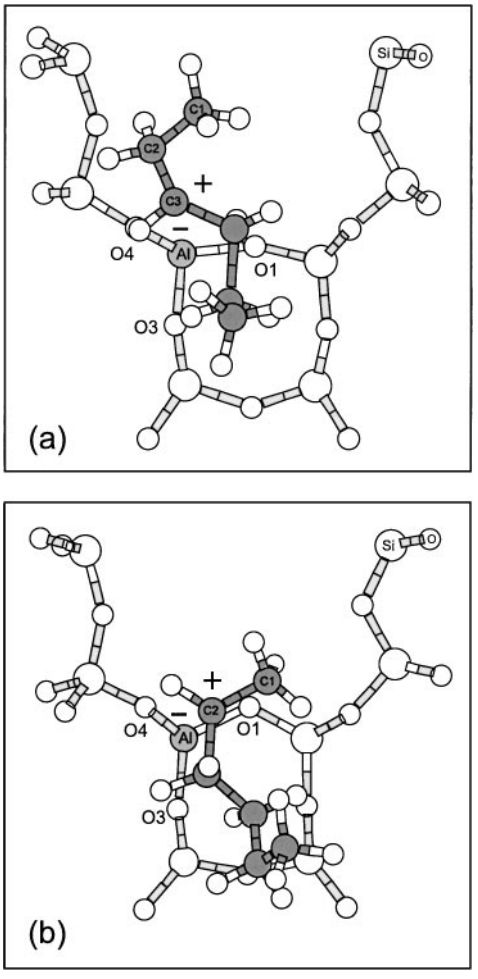

FIG. 8. Location of the protonated molecule relative to the zeolite framework and the position of the positive charge on the molecule. (a) $t = \sim 200$ fs, (b) $t = \sim 1450$ fs (cf. vertical arrows in Fig. 7).

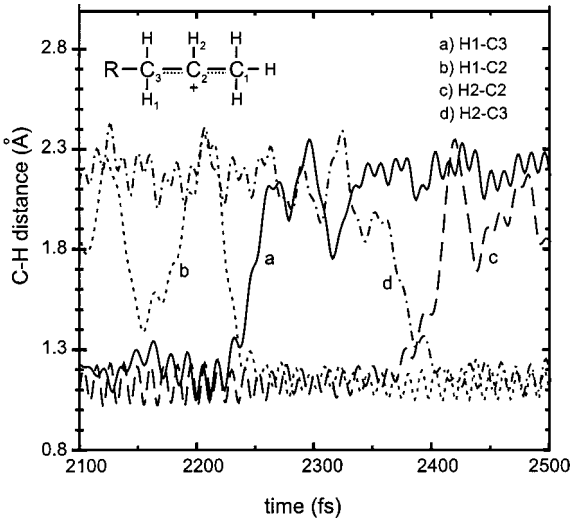

FIG. 9. Time dependence of the C–H distances illustrating two events of the hydride transfer within the protonated molecule. At ∼2230 fs H1 is transferred from C3 to C2 (a, b) and at ∼2380 fs H2 jumps from C2 to C3 (c, d).

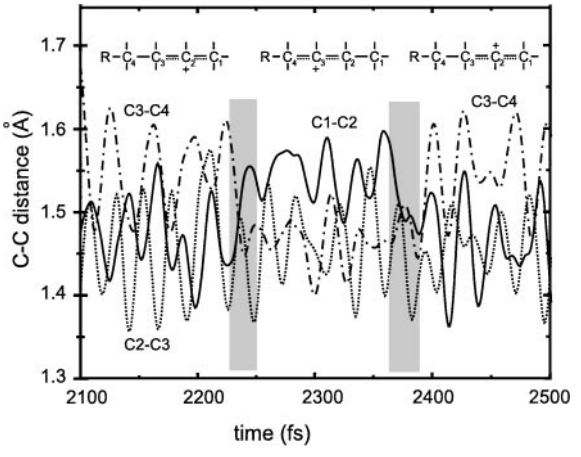

FIG. 10. Time dependence of the C–C distances. The gray areas indicate the period of the H transfer during which the C–H distance from either of the C atoms is larger than 1.2 Å.

elongated from the mean value of the double bond of ∼1.36 Å (cf. Fig. 4) to ∼1.45 Å. Gray zones in Fig. 10 indicate a period of the hydride transfer during which the distance of the H^- ion from either of the neighboring C atoms is longer than 1.20 Å. Note that upon the hydride transfer a relocation of the C–C and C–C^+ bonds occurs (cf. inset), ending with the readjustment of the C–C and C–C^+ distances.

IR spectra. Figure 11 displays simulated IR spectra of the neutral and protonated hexene molecule adsorbed in the zeolite. The C–H stretching of hexene produces an intense band centered at ∼2850 cm^{-1} similar to that of the saturated molecule (Fig. 5a). No major differences in the C–H bonding are observed for the H atoms bound to the four-coordinated neutral C atom and to the three-coordinated C^+ atom (Fig. 9). The simulated spectrum of the C–H stretching of the protonated molecule (Fig. 11b) is therefore similar to the spectra of both the nonprotonated unsaturated molecule (Fig. 11a) and the saturated

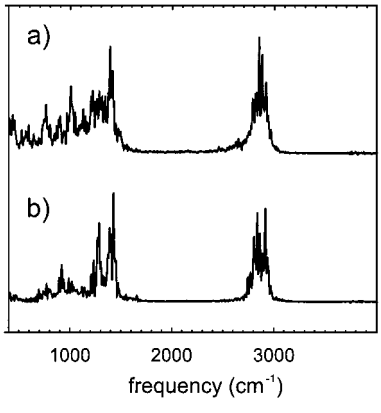

FIG. 11. Simulated spectra of neutral hexene (a) and protonated hexene (b) adsorbed in the zeolite.

molecule (Fig. 5a). All frequencies of the C–C bonding are located below 1500 cm^{-1} and are overlapped with skeletal modes of the zeolite framework. Despite distinct differences in the C–C and C–C^+ bonding displayed in Fig. 10 no clear and distinctive feature evidencing the existence of the protonated intrazeolite species is expected in the IR spectra.

5. CONCLUSIONS

First-principles short-term molecular dynamics simulations for sampling the behavior of linear hydrocarbons within an acid zeolite gmelinite at high temperature have been performed. The trajectories show periodic movement of the paraffin, indicating rather inert behavior of saturated molecules. The more complex movement of the olefins is due to slight affinity of the acid site toward the double bond.

The simulated IR spectrum of the adsorbed hydrocarbon is similar to the experimental spectrum of the molecule *in vacuo* with the broadband of the C–H stretching centered at ~2860 cm^{-1}. The spectra projected to the H atoms show that high- and low-frequency components of the C–H stretching band are due to the differences in the bonding within the CH_3 and CH_2 groups, respectively. In the simulated O–H stretching of the zeolitic acid site, a decrease of frequencies is observed upon adsorption of hydrocarbons. The estimated downshift of ~180 cm^{-1} is in reasonable agreement with available experimental data.

The high-temperature behavior of the protonated species is simulated with a linear $C_6H_{13}^+$ carbocation located within the main channel of the zeolite. Static relaxation of all atomic positions of the secondary cation placed in the channel of the negatively charged zeolite framework shows that a separation of charges is disadvantaged by ~60 kJ/mol. Several independent simulations show, however, that the protonated molecule is stabilized in the zeolite and no collapse to the neutral molecule occurs. The balanced position in the channel restricts the frequency of contacts with the framework. In this situation the probability of the back-transfer of the proton to the zeolite is low. The protonated molecule, which is a very strong acid, is thus stabilized and long-lived in the channel of a zeolite.

The protonated molecules show rather high mobility, and our simulations indicate that an electronically unbalanced bonding of the carbocation allows a deformation of the molecular skeleton much larger than that of the neutral molecules. No cracking or isomerization event, however, is observed. The movement is accompanied by a series of hydride transfer along the chain of the molecule. The transfer of the H^- ion leads to the relocation of the positive charge. The relocation is correlated with respect to the position of the Al site in the zeolite framework. Both the significant deformability of the backbone and the mobility of H atoms within the protonated species observed in our simulation agree well with numerous scenarios of chemical conversions in zeolites.

In the simulated IR spectra of protonated species we observe no distinctive feature in the C–H stretching that could serve as evidence for the existence of carbocations. The frequency range corresponding to the C–C bonding overlaps that of skeletal vibration of the zeolite and this does not make it possible to identify differences in the C–C and C–C^+ bondings observed in our simulations.

Neither the dynamics of physisorbed molecules nor that of the protonized species disclose a tendency of the linear molecules to undergo any conversion process (isomerization or cracking). A conversion is likely to happen during the period of tight contact between the molecule and a zeolite when molecules are chemisorbed and form alkoxy species. No such contacts, however, have been observed because high temperatures support removal of chemisorbed molecules from the surface. Our results thus indicate that future simulations should focus on alkoxy species. A characterization of these reaction intermediates, i.e., conditions of the formation, and a period of the lifetime will require, however, simulations at considerably lower temperatures.

ACKNOWLEDGMENTS

The work has been performed within the Groupement de Recherche Européen "Dynamique Moléculaire Quantique Appliquée à la Catalyse," founded by the Council National de la Recherche Scientifique (France), the Institut Français du Pétrole (IFP), TOTAL Recherche et Development, and the Universität Wien. Computing facilities at IDRIS (France) are kindly acknowledged.

REFERENCES

1. Ward, J. W., *in* "Zeolite Chemistry and Catalysis" (J. Rabo, Ed.), ACS Monograph 171. American Chemical Society, Washington, DC, 1976.
2. Jacobs, P. A., "Carboniogenic Activity of Zeolites." Elsevier, New York, 1977.
3. Dwyer, J., *in* "Innovation in Zeolite Material Science" (P. J. Grobet, W. J. Mortier, E. F. Vansant, and G. Schulz-Ekloff, Eds.). Elsevier, Amsterdam, 1988.
4. Haag, O., *in* "Zeolites and Related Microporous Materials: State of the Art 1994" (Studies in Surface Science and Catalysis, J. Weitkamp, H. G. Karge, H. Pfeifer, W. Hölderich, Eds.), Vol. 84, pp. 1375–1394. Elsevier, Amsterdam, 1994.
5. Tanabe, K., and Hölderich, F. W., *Appl. Catal. A* **181**, 399 (1999).
6. Whitmore, F. C., *Ind. Eng. Chem.* **26**, 94 (1934).
7. van Santen, R. A., *J. Mol. Catal. A* **115**, 405 (1997).
8. Kazansky, V. B., *Catal. Today* **51**, 419 (1999).
9. Kazansky, V. B., Frash, M. V., and van Santen, R. A., *Appl. Catal. A* **146**, 225 (1996).
10. Corma, A., and Orchillés, A. V., *Micropor. Mesopor. Mater.* **35–36**, 21 (2000).
11. Sommer, J., Jost, R., and Hachoumy, M., *Catal. Today* **38**, 309 (1997).
12. Kotrel, S., Knözinger, H., and Gates, B. C., *Micropor. Mesopor. Mater.* **35–36**, 11 (2000).
13. Allen, M. P., and Tildesley, D. J., "Computer Simulations of Liquids." Clarendon, Oxford, 1987.

14. Demontis, P., and Suffritti, G. B., *Chem. Rev.* **97**, 2845 (1997).
15. Schenk, M., Vidal, S. L., Vlugt, T. J. H., Smit, B., and Krishna, R., *Langmuir* **17**, 1558 (2001).
16. Sauer, J., Ugliengo, P., Garrone, E., and Saunders, V. R., *Chem. Rev.* **94**, 2095 (1994).
17. Campana, L., Selloni, A., Weber, J., and Goursot, A., *J. Phys. Chem. B* **101**, 9932 (1997).
18. Benco, L., Demuth, T., Hafner, J., and Hutschka, F., *Micropor. Mesopor. Mater.* **42**, 1 (2001).
19. Nusterer, E., Blöchl, P. E., and Schwarz, K., *Angew. Chem. Intern. Ed.* **35**, 175 (1996).
20. Nusterer, E., Blöchl, P. E., and Schwarz, K., *Chem. Phys. Lett.* **253**, 448 (1996).
21. Schwarz, K., Nusterer, E., Margl, P., and Blöchl, P. E., *Int. J. Quantum Chem.* **61**, 369 (1997).
22. Haase, F., Sauer, J., and Hütter, J., *Chem. Phys. Lett.* **266**, 397 (1997).
23. Stich, I., Gale, J. D., Terakura, K., and Payne, M. C., *Chem. Phys. Lett.* **102**, 7307 (1998).
24. Jeanvoine, Y., Ángyán, J. G., Kresse, G., and Hafner, J., *J. Phys. Chem. B* **102**, 7307 (1998).
25. Benco, L., Demuth, T., Hafner, J., and Hutschka, F., *Chem. Phys. Lett.* **324**, 373 (2000).
26. Benco, L., Demuth, T., Hafner, J., and Hutschka, F., *Chem. Phys. Lett.* **330**, 457 (2000).
27. Stich, I., Gale, J. D., Terakura, K., and Payne, M. C., *J. Am. Chem. Soc.* **121**, 3292 (1999).
28. Galli, E., Passaglia, E., and Zanazzi, P. F., *N. Jb. Miner. Mh.* **1982**, 1145 (1982).
29. Durà-Vilà, V., and Gale, J. D., *J. Phys. Chem. B* **105**, 6158 (2001).
30. Benco, L., Demuth, T., Hafner, J., and Hutschka, F., *J. Chem. Phys.* **111**, 7537 (1999).
31. Jones, R. O., and Gunnarsson, O., *Rev. Mod. Phys.* **61**, 689 (1989).
32. Perdew, J. P., Chevary, A., Vosko, S. H., Jackson, K. A., Peredsen, M. R., Singh, D. J., and Fiolhais, C., *Phys. Rev. B* **46**, 6671 (1992).
33. Vanderbilt, D., *Phys. Rev. B* **41**, 7892 (1990).
34. Kresse, G., and Hafner, J., *J. Phys. Cond. Matter* **6**, 8245 (1994).
35. Kresse, G., and Furthmüller, J., *Phys. Rev. B* **54**, 11169 (1996).
36. Blöchl, P. E., *Phys. Rev. B* **50**, 17953 (1994).
37. Kresse, G., and Joubert, D., *Phys. Rev. B* **59**, 1758 (1999).
38. Nosé, S., *J. Chem. Phys.* **81**, 511 (1984).
39. Patton, D. C., and Pederson, M. R., *Int. J. Quantum. Chem.* **69**, 619 (1998).
40. Snyder, J. A., Jaffe, J. E., Gutowski, K., Lin, Z., and Hess, A., *J. Chem. Phys.* **112**, 3014 (2000).
41. Benco, L., Demuth, T., Hafner, J., Hutschka, F., and Toulhoat, H., *J. Chem. Phys.* **114**, 6327 (2001).
42. Eder, F., and Lercher, J. A., *J. Phys. Chem. B* **101**, 1275 (1997).
43. Eder, F., and Lercher, J. A., *Zeolites* **18**, 75 (1997).
44. Demuth, T., Benco, L., Hafner, J., Toulhoat, H., and Hutschka, F., *J. Chem. Phys.* **114**, 3703 (2001).
45. Trombetta, M., Armaroli, T., Gutièrez Alejandre, A., Ramirez Solis, J., and Busca, G., *Appl. Catal. A: Gen.* **192**, 125 (2000).
46. Benco, L., Tunega, D., Hafner, J., and Lischka, *J. Phys. Chem. B*, in press.
47. NIST, Standard Reference Database (www.nist.gov).
48. Lercher, J. A., Gründling, C., and Eder-Mirth, G., *Catal. Today* **27**, 353 (1996).
49. Yamagishi, K., Namba, S., and Yashima, T., *J. Phys. Chem.* **95**, 872 (1991).
50. Eder, F., Stockenhuber, M., and Lercher, J. A., *J. Phys. Chem. B* **101**, 5414 (1997).
51. Haw, J. F., Nicholas, J. B., Song, W., Deng, F., Wang, Z., Xu, T., and Heneghan, C. S., *J. Am. Chem. Soc.* **122**, 4763 (2000).
52. Song, W., Nicholas, J. B., and Haw, J. F., *J. Am. Chem. Soc.* **123**, 121 (2001).